DOI: 10.31401/WS.2025.proc.18

Proceedings of
the Seventeenth Workshop “Solar Influences on the Magnetosphere, Ionosphere and Atmosphere”
June, 2025

Space Weather Influences on Satellite Anomalies

Kirov B., Georgieva K., Asenovski S.

Space Research and Technology Institute, Bulgarian Academy of Sciences, Bl.3 Acad. G. Bonchev str. 1113 Sofia, Bulgaria
bkirov@space.bas.bg

Abstract

Space weather drives on-orbit anomalies through multiple, orbit-dependent pathways. In low Earth orbit (LEO), enhanced thermospheric drag during storms, nighttime auroral charging, and galactic-cosmic-ray (GCR) single-event effects (SEE) are prominent. In geostationary orbit (GEO), surface and deep-dielectric charging—often amplified on the nightside during substorm injections—remain leading root causes. Using consolidated anomaly catalogs (Seradata/SpaceTrak aggregates, GOES operator logs) and supplemental fleet counts from UCS snapshots, we quantify anomaly occurrence per satellite-year by orbit regime and examine dependences on magnetic local time (MLT), geomagnetic activity (daily Kpmax, GFZ/WDC), and solar-cycle phase (sunspot number v2.0). Normalization by exposure shows that the daily probability of anomaly rises sharply for Kp ≥ 5, even though raw counts are larger under quiet conditions because quiet days dominate. The solar-cycle analysis reveals a pre-maximum enhancement consistent with outer-belt acceleration and cumulative MeV-electron fluence that governs internal charging, whereas a GCR-related SEE contribution in LEO partly anti-correlates with sunspot number. We synthesize these relationships into mitigation guidance: (i) design hardening (conductive/UV-stable surfaces and bonding, minimized floating dielectrics, rad-hard parts, current limiting, ECC/TMR with scrubbing); (ii) operational playbooks keyed to upstream solar-wind/SEP/electron monitors and geomagnetic indices; and (iii) calibrated forecasts/nowcasts and AE9/AP9/SPM-based specifications that map environment to anomaly likelihood by orbit and MLT. The framework provides actionable thresholds for fleet operations and transparent benchmarks for future anomaly reporting and model validation.

Keywords: Space weather; satellite anomalies; solar influences

1. Introduction

Space weather refers to the dynamic conditions in the near-Earth space environment, driven by solar activity and solar-terrestrial interactions. According to the U.S. National Space Weather Program, space weather is characterized by conditions in the solar wind, magnetosphere, ionosphere, and thermosphere affecting the performance and reliability of space-borne and ground-based technological systems (Seki et al., 2018). Its study is crucial due to its significant impact on satellite systems, potentially leading to operational anomalies, disruptions, or even loss of spacecraft]. Intense solar phenomena such as solar flares, coronal mass ejections, high-speed solar wind streams, and solar proton events, as well as persistent factors like cosmic rays and Earth's radiation belts, pose substantial risks to satellites in various orbits. Understanding these factors is critical for enhancing satellite resilience and ensuring the reliability of vital services provided by satellite infrastructure. This paper aims to provide an overview of the primary space weather factors responsible for satellite anomalies, explore the mechanisms behind these impacts, analyze the dependence of anomalies on orbital characteristics, and discuss mitigation strategies and forecasting capabilities.

2. Space Weather –Primary Factors

Space weather encompasses phenomena stemming from the Sun and the space environment, such as solar flares, coronal mass ejections (CMEs), high-speed solar wind streams (HSS), solar proton events (SPE), cosmic rays, and radiation belts (Seki et al., 2018; Kamide, 2013).

Solar flares. These sudden and intense bursts of X-ray and ultraviolet (UV) radiation from the Sun, accompanied by energetic particle emissions, significantly affect near-Earth space, causing ionospheric disturbances and enhancing high-energy proton fluxes. The ionospheric disturbances directly influence communication and navigation (Harrison et al., 2017) 9Phillips et al., 2016). A comprehensive understanding of solar flares is essential for predicting their potential impacts on communication and power grid systems.

Coronal mass ejections (CME). These massive eruptions of plasma and embedded magnetic fields from the Sun's corona, upon interacting with Earth's magnetosphere, can induce severe geomagnetic storms. These storms dramatically alter the radiation belts and magnetospheric environment, creating hazardous conditions such as induced currents and elevated particle fluxes, detrimental to satellite operations (Harrison et al., 2017).

High-speed solar wind streams (HSS). Originating from coronal holes on the solar surface, these streams, although weaker than typical CMEs, can cause prolonged, moderate geomagnetic disturbances (Harrison et al., 2017). HSS-induced substorms and increased fluxes of energetic particles lead to charge accumulation on satellite surfaces, increasing the risk of electrostatic discharges (Seki et al., 2018).

Solar proton events (SPE). High-energy proton and ion bursts accelerated by large solar eruptions or CME-driven shock waves arrive at Earth within hours. These particles can pose risks to astronauts in space and can disrupt satellite electronics, primarily through radiation damage (Crowley et al., 2010; Robinson, 2012).. SPEs significantly heighten the risk of electrical discharges and electronic component failures

Cosmic rays. Originating from beyond the Solar System, these highly energetic particles continuously bombard Earth's orbit. Despite fluctuations with the 11-year solar cycle, cosmic rays significantly contribute to single-event upsets (SEU) in satellite electronics, particularly during solar minima.

Radiation belts. Earth's Van Allen radiation belts trap high-energy electrons and protons, which intensify during solar storms. These belts pose continuous risks, especially for satellites in medium Earth orbits (MEO) and geostationary Earth orbits (GEO), due to cumulative radiation damage and frequent anomalies resulting from persistent exposure (Kamide, 2013; Harrison et al., 2017).

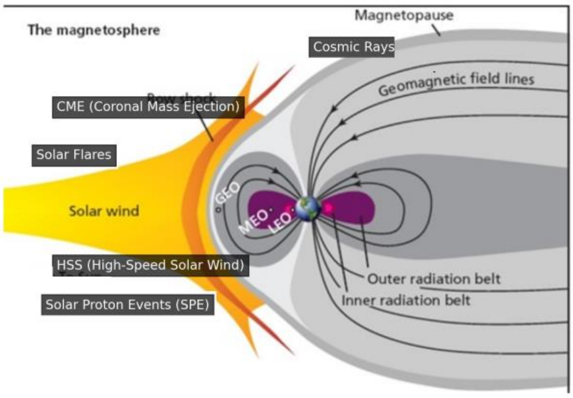

Figure 1. *Schematic of the Earth's magnetosphere, with several regions labeled wheresatellite anomalies often occur, including the Van Allen Radiation Belts (Inner andOuter), and typical satellite orbits (GEO, MEO, and LEO) and space weather factors. Courtesy of RAND Corporation, www.RAND.org.*

Regime	Description	Typical hazard
Absolute charging	The whole spacecraft floats to a nearly uniform potential (±kV). Sudden environmental changes (e.g., eclipse exit) drive large potential shifts and spark *global* electrostatic discharges (ESD).	Arcing on solar-array strings, loss of star-tracker sensitivity, momentary bus resets.
Differential charging	Local material properties and view-factors create patchy potentials (ΔV ≈ kV over cm). Strong local E-fields trigger *micro-arcs*.	Pitting of thermal blankets, antenna feed damage, sensor drop-outs.

Regime	Dominant hazards	Secondary
LEO	Drag surges; auroral surface charging; SAA-driven TID/SEEs	SEP-driven SEEs; atomic oxygen erosion
MEO	Trapped-proton TID; MeV-electron internal charging; SEEs	SEP-driven SEEs; eclipse SRP modeling errors (service impacts)
GEO	MeV-electron internal & surface charging; deep dielectric discharges	SEP-driven SEEs; cumulative dose

3. Mechanisms of Space-Weather–Driven Satellite Anomalies

Space-weather disturbances couple into spacecraft through several well-characterised physical pathways. The subsections below summarise the dominant mechanisms and illustrate how each can provoke functional anomalies or outright mission loss.

3.1 Surface Charging

Energetic electrons (∼1 eV – 30 keV) and low-energy ions in the magnetospheric plasma current to exposed spacecraft surfaces. Two regimes are distinguished:

GEO platforms are particularly vulnerable during eclipse season when the ambient electron density collapses and stored charge can suddenly discharge (Minow et al., 2024).

3.2 Deep-Dielectric (Internal) Charging

Mega-electron-volt electrons penetrate external metal and accumulate in dielectric layers (cable insulation, PCB substrates). Charge builds until the internal electric field exceeds the breakdown strength (∼200–400 kV cm^{-1}), producing a punch-through discharge that often destroys power-converter transformers, gate arrays or telemetry buses. Failures frequently cluster near equinox when GEO electron fluxes peak and when spacecraft enter/exit eclipse, rapidly altering internal temperature and resistance (Horne et al., 2025).

3.3 Single-Event Effects (SEE) in Micro-electronics

A single energetic ion, proton, or heavy GCR nucleus traversing a sensitive volume causes localised ionisation:

- Single-Event Upset (SEU) – soft-error bit flips in memory or logic.
- Latch-up (SEL) – parasitic thyristor conduction path triggers over-current and thermal runaway.
- Single-Event Burn-out/ Gate-Rupture (SEB/SEGR) – catastrophic failure of power MOSFETs and GaN HEMTs.

SEE rates scale with the integral >10 MeV proton flux for LEO and with GCR flux modulated by the heliospheric cycle for GEO. Fault-tolerant design tactics include triple-modular redundancy, error-correcting memory, periodic configuration scrubbing in FPGAs, and current-limiting circuitry (Jun et al., 2024).

3.4 Enhanced Atmospheric Drag (LEO)

During strong geomagnetic storms Joule heating and particle precipitation expand the thermosphere, increasing neutral density at 200–600 km by factors of 2–10. The resulting drag torque can:

- Decrease orbital altitude and lifespan.
- Perturb attitudes on 3-axis–stabilised microsats that lack momentum margin.
- Compromise planned phasing of constellation planes.

The loss of ~40 Starlink satellites launched on 3 February 2022—during only a moderate storm (Dst ≈ –80 nT)—is the canonical recent example (Ahmad et al., 2025).

3.5 Service-Level Impacts on Communications and Navigation

Although not always recorded as spacecraft "anomalies," disturbed upper-atmosphere and solar radio conditions degrade space-based services:

- GNSS positioning errors (L-band code-phase scintillation, cycle slips, and TEC gradients) rise by an order of magnitude during post-sunset equatorial plasma bubbles and auroral substorms (Gómez Socola et al., 2025; Tahir et al., 2024).
- Tele-com links suffer carrier-to-noise degradations when solar radio bursts (Type II/IV) coincide with Earth-pointing ground-station geometry.

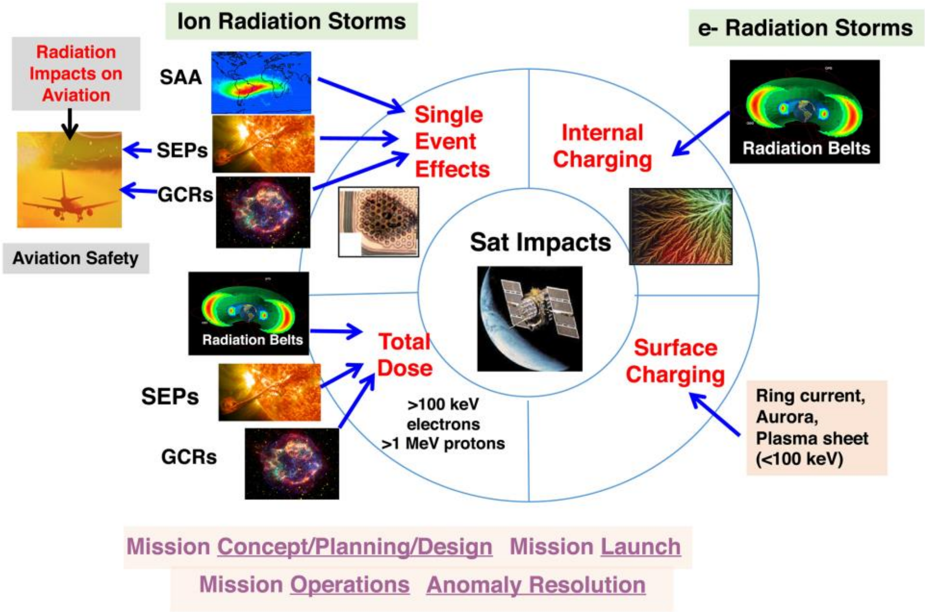

Figure 2. *Space Radiation and Plasma Effects on Satellites and Aviation (Yihua Zheng et al. 2019).*

4. Orbit Dependence

Space-weather impacts vary systematically with orbital regime and inclination because the ambient plasma, radiation, and neutral density fields change with L-shell, magnetic latitude, and local time.

4.1 Orbit type (altitude)

LEO spacecraft are most exposed to thermospheric drag enhancements during storms (Section **3**.4) and to auroral-region surface charging on high-latitude passes. Charging events >100 V negative are routinely observed during auroral crossings and correlate with geomagnetic activity. Single-event effects (SEEs) in LEO spike during SEP events; exposure is strongly inclination dependent (see §4.2). South Atlantic Anomaly (SAA) passages add trapped-proton dose and SEE risk.

MEO (GNSS ltitudes, L≈3–6). MEO platforms traverse the heart of the radiation belts and see persistent trapped protons (inner belt) and MeV electrons (outer belt), leading to higher cumulative dose and frequent SEEs relative to LEO. Dedicated monitors on Beidou/GNSS MEO spacecraft report in-situ SEUs that track the local LET/proton environment, underscoring the operational SEE hazard for navigation constellations. Extreme events can measurably degrade power subsystems and increase anomaly likelihood.

GEO (~35,786km). GEO sits on the outer-belt periphery and is continuously subject to keV–MeV electron storms; internal dielectric charging and surface charging dominate anomaly statistics. Multiple studies show strong correlations between GEO anomalies and enhancements of E>2 MeV electron fluence; classic analyses identified internal-charging signatures with 2-day fluence metrics.

Summary (by dominant risks).

Recent cross-regime statistics (2010–2022) confirm that GEO anomaly occurrence is most sensitive to relativistic-electron activity, whereas LEO anomalies align more with geomagnetic indices and local particle enhancements; MEO anomalies are tightly linked to persistent belt populations.

4.2 Inclination (magnetic latitude exposure)

Polar/high-inclination LEO. Frequent transits of the auroral oval expose spacecraft to precipitating electrons/ions and strong field-aligned currents, increasing surface-charging events and ESD risk; charging levels and anomaly counts rise with geomagnetic activity.

Equatorial/low-inclination LEO. Reduced auroral exposure but regular SAA crossings yield higher trapped-proton dose and SEEs concentrated along the SAA track.

Inclined MEO (GNSS). Typical GNSS inclinations (~55°) sweep broad magnetic latitudes, sampling both inner-belt protons and outer-belt electrons; on-board monitors show SEU occurrences that co-vary with local LET/proton spectra and storm-time electron enhancements.

GEO (near-equatorial inclination). Even with small inclinations, GEO local-time geometry matters: near-midnight to dawn sectors and eclipse seasons coincide with enhanced surface/internal charging and higher anomaly likelihood due to cold-plasma depletion and rapid environmental transitions.

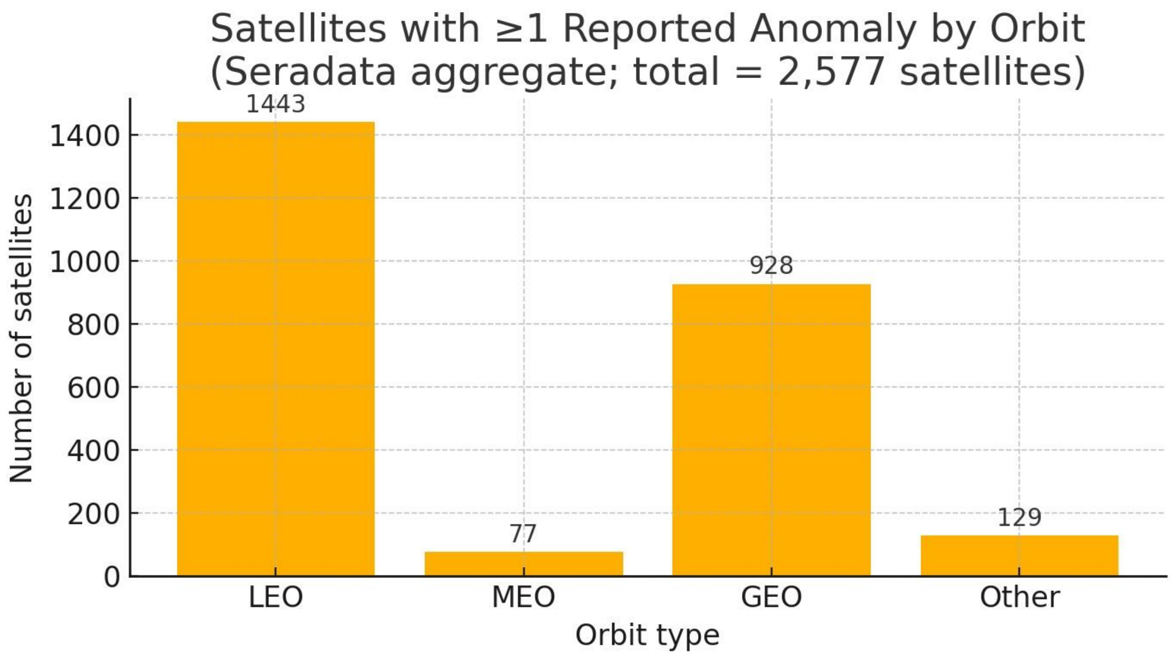

Figure 3. *Number of spacecraft with ≥1 reported on-orbit anomaly by orbit regime. Totals: LEO = 1,443, GEO = 928, MEO = 77, Other/HEO = 129 (N = 2,577). Percentages are 56%, 36%, 3%, and 5%, respectively. "Other" groups highly elliptical, transfer, and miscellaneous non-LEO/MEO/GEO orbits. Counts are per* ***spacecraft*** *(whether single or multiple events), not per* ***event****. Source: Seradata/SpaceTrak anomaly database, aggregated as in Buitrago-Leiva et al. (2024).*

It seems that MEO orbits are much more reliable than others, but this is not the case. There are several reasons why there are far fewer anomalies in databases with satellites flying on MEOs than those in other orbits.

Population effect (denominator). The global MEO fleet is tiny compared with LEO (thousands) and smaller than GEO (hundreds). Even with similar per-satellite risk, the absolute count of MEO spacecraft with ≥1 recorded anomaly will be much lower.

Reporting bias. Most MEO spacecraft are GNSS (GPS, GLONASS, Galileo, BeiDou). Their operators (often military/state) publish fewer on-orbit anomaly details. Well-known GNSS "events" (e.g., Galileo 2019, GLONASS 2014) were largely ground-segment or service issues and typically aren't logged as spacecraft anomalies in public databases.

Hardening and autonomy. GNSS platforms are built conservatively: rad-hard parts, TMR/ECC, periodic scrubbing, tight current limiting, and robust FDIR. Many radiation-induced upsets get corrected onboard and never escalate to a recorded "anomaly."

Environment vs outcome. MEO sits in a tough radiation environment (inner-belt protons + outer-belt electrons), but the design margins and operational practices keep many effects below the threshold of "reportable anomaly." So the true event rate (e.g., SEUs) can be non-trivial, while the anomaly count that reaches public logs stays small.

5. Dependence on Local Time and Geomagnetic Activity

5.1 Local time (day/night geometry and MLT sector)

GEO eclipse seasons and day–night transitions. Near the equinoxes, geostationary satellites enter Earth's shadow around local midnight. Eclipse exit brings rapid illumination changes and steep photoelectron/current gradients across surfaces and harnesses, which promote differential charging and ESD. GEO surface-charging anomalies show a marked night–pre-dawn preference (~21–06 MLT), consistent with substorm-driven injections on the nightside [Ferguson et al., 2011; Matéo-Vélez et al., 2018; Horne et al., 2013]. Clustering of anomalies around eclipse seasons has been reported in GEO anomaly catalogs [Iucci et al., 2005; Choi et al., 2011].

Substorms and nightside GEO. Many GEO anomalies concentrate on the nightside when injections of 10–100 keV electrons from the magnetotail are most frequent. Statistical studies link the local-time dependence (night-sector maxima) to these injections rather than to sunspot number [Iucci et al., 2005; Choi et al., 2011].

LEO auroral crossings (polar orbits). In LEO, large negative surface potentials and ESD risk arise predominantly during nighttime auroral traversals, where precipitating keV electrons and low photoemission drive negative charging (>100 V). Long-term DMSP statistics show thousands of such charging events with strong local-time/auroral dependence and enhanced occurrence during substorms and at lower solar activity [Anderson, 2012]. Event-based diagnosis of LEO anomalies also finds that many cases coincide with enhanced 30–100 keV electron fluxes and magnetic perturbations near the anomaly time [Ahmad et al., 2018].

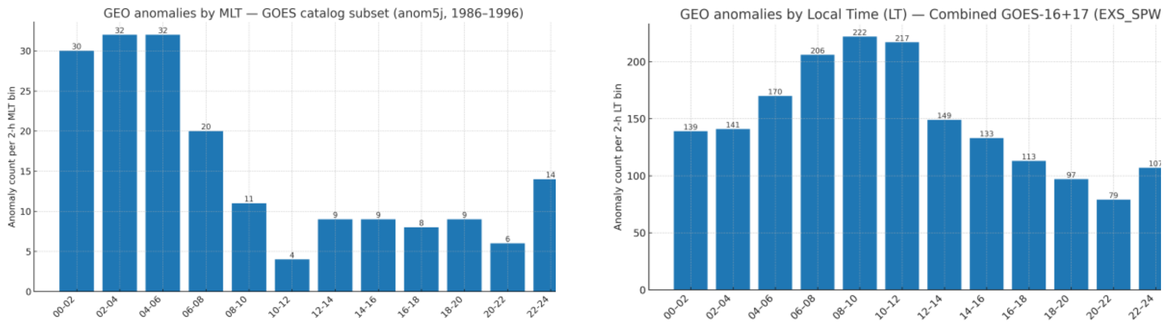

Figure 4. *GEO anomalies by Magnetic Local Time (MLT). (a) Catalog-based GEO anomalies from the legacy GOES subset (anom5j, 1986–1996): nightside/pre-dawn maximum consistent with charging/substorm injections. (b) GOES-16/17 EXIS SpaceWire (EXS_SPW) event set: instrument-specific dayside enhancement; not representative of canonical GEO charging statistics. Sources: (a) NOAA/NCEI legacy 'anom5j' GOES table; (b) GOES-16/17 EXS_SPW engineering logs.*

5.2 Geomagnetic-activity dependence (by orbit)

GEO. The strongest statistical link is with relativistic/MeV electrons that charge internal dielectrics (deep dielectric charging). GEO anomalies correlate with the integrated >2 MeV electron fluence over the preceding ~1–2 days, not with sunspot number; the relationship strengthens during storm/substorm activity and near the equinoxes [Wrenn, 1995; Choi et al., 2011; Meredith et al., 2015; Minow et al., 2024].

LEO. Anomaly occurrence increases with auroral electron precipitation and geomagnetic disturbance (e.g., elevated AE/Kp), with a pronounced nightside dependence and frequent proximity to substorms. During solar minima, GCR-related SEE can also be relatively elevated, contributing to logic upsets even under low Kp conditions [Anderson, 2012; Ahmad et al., 2018; Iucci et al., 2005].

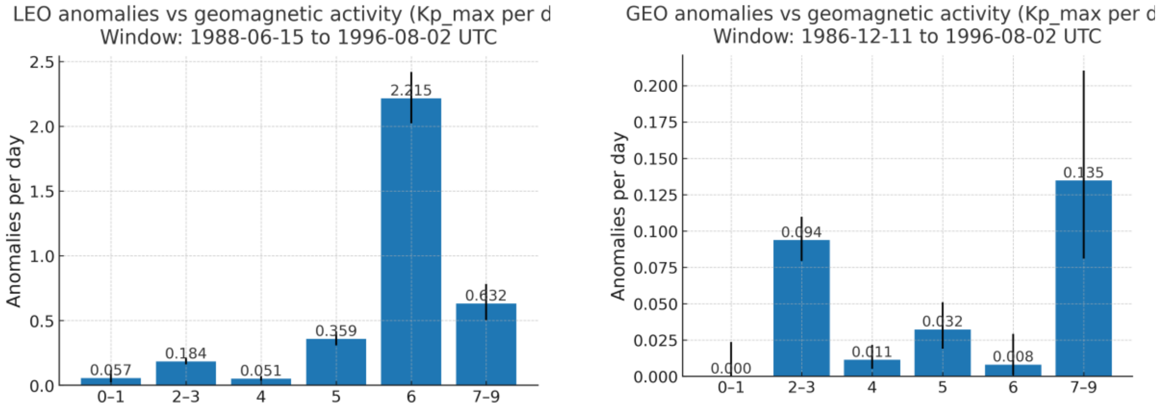

Figure 5. *Anomaly rate vs geomagnetic activity (daily Kp_max). (a) LEO anomalies (ALT ≤ 2000 km), 1988-06-15 to 1996-08-02 UTC. (b) GEO anomalies (GOES legacy list), 1986-12-11 to 1996-08-02 UTC. Bars show anomalies per day by Kp bin (0–1, 2–3, 4, 5, 6, 7–9) with 95% Poisson confidence intervals (Byar). Data sources: Daily Kp_max — GFZ/WDC (Matzka et al., 2021; doi:10.5880/Kp.0001). Anomaly catalogs — LEO from anom5j.xlsm (ALT ≤ 2000 km), GEO from GoesAnomalyTrends.xlsm.*

MEO (GNSS). MEO satellites traverse the heart of the belts; while the environment is severe, platform hardening and operations often suppress reportable anomalies. Where on-board monitors are available (e.g., BeiDou), SEE activity and LET spectra track radiation conditions, while relativistic-electron fluxes at GPS-type L-shells peak during enhanced geomagnetic activity [Meredith et al., 2016; Zhang et al., 2023; Ye et al., 2021]. Consequently, MEO anomaly rates may show mixed dependence: internal-charging/SEE components strengthening with geomagnetic disturbances and GCR-driven SEE showing anti-correlation with solar activity.

6. Dependence on solar-cycle phase (sunspot number)

Solar-cycle modulation of satellite anomalies arises from how solar activity controls the drivers of the near-Earth radiation environment. During active phases, coronal mass ejections (CMEs) and high-speed streams (HSS) trigger geomagnetic storms and substorms. These, in turn, heat and expand the thermosphere (raising LEO drag), inject and accelerate keV–MeV electrons (enhancing surface charging in LEO/GEO and deep-dielectric charging at GEO), and elevate solar energetic proton (SEP) fluxes that increase single-event effects (SEE). Hence, higher sunspot number (SSN) generally implies a higher likelihood of anomalies through these pathways—though the response is orbit-dependent and not strictly proportional to SSN [Wrenn et al., 2002; Meredith et al., 2015; Baker et al., 2018].

Crucially, the geoeffective particle environment does not peak exactly with SSN. At GEO, anomaly statistics correlate best with the integrated fluence of >2 MeV electrons over the prior 1–2 days—a quantity that often maximizes in the rising and declining phases when chorus-driven acceleration and storm-time injections are strongest, rather than at SSN peak [Wrenn et al., 2002; Meredith et al., 2015; Baker et al., 2018]. In LEO, nightside auroral charging and substorm activity can be frequent under modest to strong driving, while GCR-driven SEE anti-correlates with SSN and becomes relatively more important toward solar minima [Buitrago-Leiva et al., 2024; Baker et al., 2018].

Figure ***6*** compares the annual anomaly rate per satellite-year for LEO and GEO with the annual SSN (SILSO v2.0). The curves reveal a pre-maximum enhancement in anomalies during Solar Cycle 24. This is consistent with intense storm sequences and equinoctial coupling in 2011–2012 that produced large seed and relativistic electron populations. Note also that Solar Cycle 24 exhibited a double maximum (∼2012 and ∼2014); the first peak is partially obscured by annual averaging/smoothing in the SSN curve, but the anomaly rate retains a clear rise on the early-maximum flank [Reeves et al., 2013; Wrenn et al., 2002; Meredith et al., 2015].

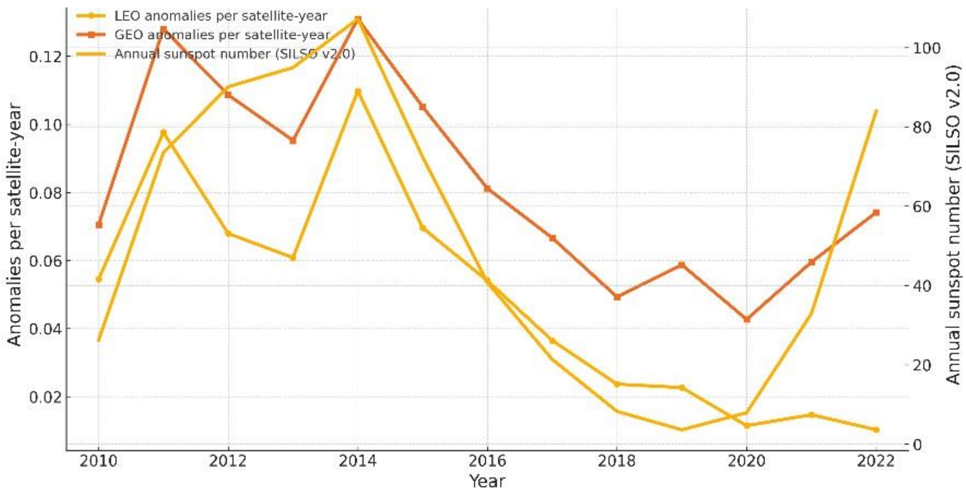

Figure 6. *LEO and GEO anomalies per satellite-year vs annual sunspot number (2010–2022). Anomaly rates (left axis) derive from the Seradata/SpaceTrak anomaly compilation aggregated in [Buitrago-Leiva et al., 2024] and normalized by annual fleet size (UCS Satellite Database, 2020–2023 snapshots, interpolated to 2010–2019). Sunspot number (right axis): WDC-SILSO v2.0 (DOI: 10.24414/qnza-ac80). Rates peak on the rising/declining flanks rather than at SSN maximum, reflecting storm-time seed/MeV electron enhancements (GEO internal charging) and mixed LEO contributions (auroral charging, SEP-related SEE, and GCR-related SEE). Cycle-dependent changes in CME and heliospheric pressures can modulate CME expansion and geoeffectiveness, providing additional context for anomaly peaks near solar maxima [Gopalswamy et al., 2024].*

7. Mitigation and Forecasting Strategies

7.1 Design hardening and materials (charging, radiation)

Design begins with making the environment non-catastrophic for the hardware. For surface and internal charging, best practice includes low-resistivity/UV-stable coatings, controlled ground paths and bonding, avoidance of isolated dielectrics, and placing sensitive harnesses behind conductive structure. For internal charging, designers allocate dielectric thickness, leakage paths, and shielding such that worst-case internal dose rates keep electric fields below breakdown margins; GEO is most demanding. Rad-hard parts, part derating, current-limiting and latch-up protection, ECC/TMR with periodic memory scrubbing, and watchdog/safe-hold logic reduce the probability that single-event effects escalate to anomalies [Minow et al., 2024; Matéo-Vélez et al., 2018; Wrenn, 1995; Wrenn et al., 2002; NASA-HDBK-4002B, 2022; NASA-STD-4005A, 2016; NASA-HDBK-4006A, 2024].

7.2 Fault management and operational playbooks

Operational risk can be cut substantially by conditioning the spacecraft state on upstream warnings and local monitors. Common measures include: pre-emptive safe-mode entry; powering down high-voltage or non-essential loads; biasing attitudes to reduce differential charging; delaying propulsion or sensitive payload operations; and raising error-correction/scrubbing cadence. Thresholds are typically tied to SEP and electron flux monitors (e.g., GOES), geomagnetic indices (Kp/AE), or solar-wind–derived coupling proxies; these actions are most effective when applied hours before the peak response [Choi et al., 2011; Iucci et al., 2005; Horne et al., 2021; Newell et al., 2007].

7.3 Environment specification and design margins

To dimension shielding and set charging/radiation margins, modern environment specifications rely on AE9/AP9/SPM for trapped particles with quantified uncertainties, replacing legacy AE8/AP8; internal-charging design should use fluence/flux percentiles from these models rather than climatological means. For LEO drag risk, thermospheric density models (e.g., NRLMSISE-00) and density climatologies inform conjunction with orbit-maintenance margins and power/thermal budgets [Ginet et al., 2013; Picone et al., 2002; Emmert, 2015].

7.4 Forecasting and nowcasting for operations

Short-lead alerts combine (i) solar-wind measurements at L1 (DSCOVR/ACE) with (ii) empirical/physics-based drivers of geomagnetic response (e.g., the Newell coupling function) to anticipate geomagnetic activity for GEO/LEO charging and MEO radiation risk. For relativistic electrons, skillful GEO nowcasts/forecasts feed into anomaly likelihood for internal charging; for LEO drag, atmospheric models driven by solar/EUV proxies are used for maneuver planning. Probabilistic forecasts with explicit uncertainty are increasingly recommended, and machine-learning methods are being fused with physics-based models to provide actionable risk metrics for operators [Horne et al., 2021; Newell et al., 2007; Emmert, 2015; Camporeale, 2019].

7.5 Fleet-level risk management

Large constellations benefit from statistically calibrated hazard-to-risk mappings: anomaly-per-satellite-day as a function of Kp/AE and local time, and orbit-class-specific thresholds for deep-dielectric charging and SEE. Rolling A/B tests (e.g., increased scrubbing or bias changes) during elevated activity quantify mitigation benefit. Combining design hardening, operational playbooks, and calibrated forecasts yields the largest reduction in anomaly rates at minimal cost [Hands et al., 2018; Horne et al., 2021]. Radiation-risk assessment that couples in-flight dosimetry with numerical transport is routinely used beyond Earth orbit and informs design/operations trade-offs [Krastev et al., 2024].

8. Conclusions

Space weather drives satellite anomalies through multiple, orbit-dependent pathways. In LEO, enhanced thermospheric drag during storms, nighttime auroral charging, and GCR-driven single-event effects (SEE) dominate. In GEO, deep-dielectric and surface charging—often amplified on the nightside during substorm injections—remain the leading root causes. MEO platforms reside in a severe radiation environment, yet public anomaly catalogs under-report spacecraft-level events relative to LEO/GEO because of hardening, autonomy, and reporting practices. Across the aggregated sample ($N \approx 2,577$ spacecraft with ≥ 1 reported anomaly), the distribution by orbit class is strongly skewed toward LEO (≈56%) and GEO (≈36%), with far fewer MEO and HEO/other cases—reflecting both environmental exposure and population/reporting effects.

Local-time and geomagnetic-activity dependences are clear. GEO anomalies cluster on the night/pre-dawn sector, consistent with injections of 10–100 keV electrons from the magnetotail that drive surface and internal charging. LEO anomalies occur preferentially during nighttime auroral traversals, when photoemission is weak and precipitating electrons elevate charging risk. When normalized by exposure (days in each Kp bin), the probability of anomaly per day increases with geomagnetic activity—especially for Kp ≥ 5—despite raw counts appearing larger at low Kp simply because quiet days are far more common.

Solar-cycle modulation is evident in the anomaly-per-satellite-year metrics. GEO-like charging risks track the build-up of relativistic/MeV electrons, yielding peaks near (and sometimes slightly before) sunspot maxima, consistent with outer-belt acceleration and the cumulative fluence that governs deep-dielectric charging. In contrast, LEO SEE components include a GCR contribution that tends to anti-correlate with solar activity, partly offsetting storm-time increases in auroral-charging-related events. These phase differences—and the well-known "double maxima" in some solar cycles—help explain the observed pre-maximum bump in anomalies.

Implications for design and operations. The most effective risk reduction comes from combining (i) design hardening (conductive/UV-stable surfaces, managed grounds/bonds, minimized floating dielectrics, rad-hard parts, current limiting, ECC/TMR with scrubbing), (ii) operational playbooks keyed to upstream solar-wind/SEP/electron monitors and geomagnetic indices (pre-emptive safe-modes, HV stand-downs, attitude/bias adjustments, schedule deferrals), and (iii) calibrated forecasts/nowcasts that map environmental drivers to anomaly likelihood by orbit and local time. Using modern specifications (e.g., AE9/AP9/SPM percentiles for trapped particles; validated density models for LEO drag) aligns margins with true tail risks rather than climatological means.

Limitations and data needs. Catalog-based results still carry biases: incomplete or uneven reporting (notably in MEO), ambiguous time tags for some events, and the use of LT as a proxy for MLT in parts of the historical record. Standardizing anomaly taxonomies, preserving precise timing/MLT stamps, and publishing aggregated, de-identified spacecraft-level outcomes would materially improve the fidelity of hazard-to-risk relationships.

Outlook. As fleets scale, probabilistic, orbit- and MLT-conditioned risk metrics (e.g., anomalies per satellite-day vs. Kp/AE) should become standard for mission assurance and operations. Paired with targeted hardening and pre-planned responses, such metrics can reduce anomaly rates substantially at modest cost, while enabling transparent, testable performance commitments for both operators and service users.

References

Ahmad, N., Kim, H., Kim, J., Kim, S. (2018). Diagnosing low Earth orbit satellite anomalies using NOAA-15 electron data associated with geomagnetic perturbations, *Earth, Planets and Space*, Vol. 70, 161, DOI: 10.1186/s40623-018-0852-2.

Ahmad, N., Kilowasid, L.M.M., Fakhrurroja, H., et al. (2025). How geomagnetic storms affect the loss of Starlink satellites in February 2022?, *Earth, Planets and Space*, Vol. 77, 2, DOI: 10.1186/s40623-024-02124-2.

Anderson, P.C., et al. (2012). Characteristics of spacecraft charging in low Earth orbit, *Journal of Geophysical Research: Space Physics*, Vol. 117, A01214, DOI: 10.1029/2011JA016875.

Baker, D.N., Kanekal, S.G., Hoxie, V.C., et al. (2018). Space weather effects in the Earth's radiation belts, *Space Science Reviews*, Vol. 214, 17, DOI: 10.1007/s11214-017-0452-7.

Camporeale, E. (2019). The challenge of machine learning in space weather: Nowcasting and forecasting, *Space Weather*, Vol. 17, No. 8, pp. 1166–1207, DOI: 10.1029/2018SW002061.

Choi, H.-S., et al. (2011). Analysis of GEO spacecraft anomalies: Space weather relationships, *Space Weather*, Vol. 9, S06001, DOI: 10.1029/2010SW000597.

Crowley, G., Guhathakurta, M., Oh, S., Tobiska, W. (2010). Space weather gets real—on smartphones, *Space Weather*, Vol. 8, No. 10, DOI: 10.1029/2010SW000619.

Emmert, J.T. (2015). Thermospheric mass density: A review, *Advances in Space Research*, Vol. 56, No. 5, pp. 773–824, DOI: 10.1016/j.asr.2015.05.038.

Ferguson, D.C., Denig, W.F., Rodriguez, J.V. (2011). Plasma conditions during the Galaxy 15 anomaly and the possibility of ESD from subsurface charging, *AIAA 2011–1061*, DOI: 10.2514/6.2011-1061.

Ginet, G.P., O’Brien, T.P., Huston, S.L., et al. (2013). AE9, AP9 and SPM: New models for specifying the trapped energetic particle and space plasma environment, *Space Science Reviews*, Vol. 179, pp. 579–615, DOI: 10.1007/s11214-013-9964-y.

Gopalswamy, N., Akiyama, S., Yashiro, S., Mäkelä, P., Xie, H., Michalek, G. (2024). The backreaction of the reduced heliospheric pressure on CMEs and its implications for the strength of Solar Cycle 25, *Proceedings of the Sixteenth Workshop “Solar Influences on the Magnetosphere, Ionosphere and Atmosphere”*, pp. 9–17, DOI: 10.31401/WS.2024.proc.2.

Harrison, R., Davies, J., Biesecker, D., Gibbs, M. (2017). The application of heliospheric imaging to space weather operations: Lessons learned from published studies, *Space Weather*, Vol. 15, No. 8, pp. 985–1003, DOI: 10.1002/2017SW001633.

Horne, R.B., Glauert, S.A., Meredith, N.P., Boscher, D., Maget, V., Heynderickx, D., Pitchford, D. (2013). Space weather impacts on satellites and forecasting the Earth’s electron radiation belts with SPACECAST, *Space Weather*, Vol. 11, No. 4, pp. 169–186, DOI: 10.1002/swe.20023.

Horne, R.B., Meredith, N.P., Grew, R.S., et al. (2025). Satellite internal charging for a reasonable worst-case, *Space Weather*, Vol. 23, e2024SW004226, DOI: 10.1029/2024SW004226.

Iucci, N., Levitin, A.E., Belov, A.V., Eroshenko, E.A., Ptitsyna, N.G., Villoresi, G., et al. (2005). Space weather conditions and spacecraft anomalies in different orbits, *Space Weather*, Vol. 3, S01001, DOI: 10.1029/2003SW000056.

Jun, I., Garrett, H.B., Dyer, C., et al. (2024). A review on radiation environment pathways to impacts: Radiation effects, relevant empirical environment models, and future needs, *Advances in Space Research*, Vol. 80, No. 2, pp. 215–247, DOI: 10.1016/j.asr.2024.03.079.

Kamide, Y. (2013). Space weather: Japanese perspectives, in *Geophysical Monograph Series*, Vol. 125, pp. 59–64, DOI: 10.1029/gm125p0059.

Krastev, K., Semkova, J., Koleva, R., Benghin, V., Drobyshev, S. (2024). An assessment of the radiation risk in orbit around Mars, based on measurements by the Lyulin instrument and numerical simulations, *Proceedings of the Sixteenth Workshop “Solar Influences on the Magnetosphere, Ionosphere and Atmosphere”*, pp. 83–88, DOI: 10.31401/WS.2024.proc.12.

Matzka, J., Stolle, C., Yamazaki, Y., et al. (2021). The geomagnetic Kp index and derived indices, *GFZ Data Services*, DOI: 10.5880/Kp.0001.

Meredith, N.P., Horne, R.B., Anderson, R.R. (2015). Extreme relativistic electron fluxes at geosynchronous orbit: 1996–2012, *Space Weather*, Vol. 13, No. 3, pp. 170–184, DOI: 10.1002/2014SW001143.

Meredith, N.P., Horne, R.B., Isles, J.D., Ryden, K.A., Hands, A.D.P., Heynderickx, D. (2016). Extreme internal charging currents in medium Earth orbit: Analysis of SURF plate currents on Giove-A, *Space Weather*, Vol. 14, pp. 578–591, DOI: 10.1002/2016SW001404.

Minow, J.I., Jordanova, V.K., Pitchford, D., Ganushkina, N.Y., Zheng, Y., Delzanno, G.L., Jun, I., Kim, W. (2024). ISWAT spacecraft surface charging review, *Advances in Space Research*, in press, DOI: 10.1016/j.asr.2024.08.058.

NASA-HDBK-4002B. (2022). *Avoiding problems caused by spacecraft on-orbit internal charging effects*, NASA Technical Handbook. (No DOI).

NASA-HDBK-4006A. (2024). *Low Earth orbit spacecraft charging design handbook (Revalidated 2024)*, NASA Technical Handbook. (No DOI).

NASA-STD-4005A. (2016). *Low Earth orbit spacecraft charging design standard*, NASA Technical Standard. (No DOI).

Newell, P.T., Sotirelis, T., Liou, K., Meng, C.-I., Rich, F.J. (2007). A nearly universal solar wind–magnetosphere coupling function inferred from 10 magnetospheric state variables, *Journal of Geophysical Research: Space Physics*, Vol. 112, A01206, DOI: 10.1029/2006JA012015.

Picone, J.M., Hedin, A.E., Drob, D.P., Aikin, A.C. (2002). NRLMSISE-00 empirical model of the atmosphere: Statistical comparisons and scientific issues, *Journal of Geophysical Research: Space Physics*, Vol. 107, No. A12, 1468, DOI: 10.1029/2002JA009430.

Reeves, G.D., Spence, H.E., Henderson, M.G., et al. (2013). Electron acceleration in the heart of the Van Allen radiation belts, *Science*, Vol. 341, pp. 991–994, DOI: 10.1126/science.1237743.

Robinson, R. (2012). Research to operations: Space weather's valley of opportunity, *Space Weather*, Vol. 10, No. 10, DOI: 10.1029/2012SW000854.

Seki, D., Ueno, S., Isobe, H., Otsuji, K., Cabezas, D., Ichimoto, K., et al. (2018). Space weather prediction from the ground: Case of CHAIN, *Sun and Geosphere*, Vol. 13, No. 2, pp. 157–161.

Tahir, A., Zhang, Y., Li, M., et al. (2024). Multi-instrument observation of the ionospheric irregularities and disturbances during the 23–24 March 2023 geomagnetic storm, *Remote Sensing*, Vol. 16, No. 9, 1594, DOI: 10.3390/rs16091594.

UCS Satellite Database. (n.d.). *Union of Concerned Scientists Satellite Database*. Available at: https://www.ucsusa.org/resources/satellite-database.

Wrenn, G.L. (1995). Conclusive evidence for internal dielectric charging anomalies on geosynchronous communications spacecraft, *Journal of Spacecraft and Rockets*, Vol. 32, pp. 514–520, DOI: 10.2514/3.26645.

Wrenn, G.L., Rodgers, D.J., Ryden, K.A. (2002). A solar cycle of spacecraft anomalies due to internal charging, *Annales Geophysicae*, Vol. 20, pp. 953–956, DOI: 10.5194/angeo-20-953-2002.

Ye, Y.-G., Zou, H., Zong, Q.-G., Chen, H.-F., Zou, J.-Q., Shi, W.-H., et al. (2021). Energetic electron detection packages on board Chinese navigation satellites in MEO, *Earth and Planetary Physics*, Vol. 5, No. 2, pp. 158–179, DOI: 10.26464/epp2021021.

Zhang, B., Zhang, S., Shen, G., Quan, L., Tian, C., Hou, D., Zhou, P., Ji, W. (2023). Monitor of the single event upsets and linear energy transfer of space radiation on the BeiDou navigation satellites, *Open Astronomy*, Vol. 32, No. 1, pp. 206–216, DOI: 10.1515/astro-2022-0206.

Zheng, Y., Sibeck, D.G., Reeves, G.D., et al. (2019). Space radiation and plasma effects on satellites and aviation: Quantities and metrics for tracking performance of space weather environment models, *Space Weather*, Vol. 17, No. 10, pp. 1384–1403, DOI: 10.1029/2018SW002042.